Fifth International Conference on CFD in the Process Industries
CSIRO, Melbourne, Australia
13-15 December 2006

USING CFD TO REDUCE COMMISSIONING TIME FOR ELECTROSTATIC PRECIPITATORS

R.J Haywood[1], G.J. Brown[2], L.J. Irons[1], M. Stark[3]
[1] Hatch, Brisbane, QLD [2] Alcoa World Alumina, Kwinana, WA
[3] Fowlerex Technologies Pty, Sydney, NSW

ABSTRACT

The standard procedure for the setup of airflow distribution plates within electrostatic precipitators (ESP's) typically requires a time consuming trial and error method based on repeated field measurement, followed by production interruptions for adjustment. During the recent Pinjarra Efficiency Upgrade project, Alcoa and Hatch utilized CFD analysis of the inlet flow and distribution system in two new alumina calciner ESP's to eliminate the need for field adjustment, thereby significantly shortening commissioning time and costly production delays.

NOMENCLATURE

C_C contraction coefficient
P pressure
K momentum loss coefficient
V velocity

ε porosity
ρ density

INTRODUCTION

A recent upgrade project at Alcoa's Pinjarra Refinery has targeted a wide range of process and environmental improvements including the addition of ESP's as the preferred option for gas cleaning. The upgrade project has made provision for a total of 4 new units to be installed and operational by November 2006.

ESP's are well accepted and widely used for air pollution control due to reasonable collection efficiency, low pressure-drop, and low capital and operating costs. The performance of modern ESP's would be expected to be better than 99.9% particulate removal efficiency while incurring less than 100 Pa pressure drop. Although commercially available ESP's for large scale industrial gas cleaning exhibit slight variations in design characteristics, componentry, and mechanical cleaning style, all achieve gas cleaning quite simply by the use of electrostatic forces acting on airborne solid particles to promote their attraction to and eventual collection on charged electrodes. Maximising the time available for particulate to migrate to collection surfaces and minimising the likelihood of solids re-entrainment dictates that the collection efficiency of ESP's is strongly dependent on achieving a uniform and low-velocity gas-flow throughout the main body of the ESP within inter-electrode passages. Hence, considerable care must be exercised in the design of supply ductwork and flow conditioning upstream of the ESP.

One method for achieving an acceptable internal flow is through the use of a "Gas Distributor Plate" (GDP) which covers the complete inlet cross section of the ESP main body and is comprised of an array of plates with a W shaped cross section with 110 x 120 mm rectangular openings on a square pitch of 250 mm. Additional W shaped plates (called "zig-zag" plates) with the same design, slide laterally on the main array to provide local closure of the apertures to a minimum size of 110 mm x 60 mm (50% of the normal open area). The resistance of the GDP generally and the ability to reduce locally the effective porosity by adjustment of zig-zag plates provides the means to make field adjustments to the gas flow distribution and optimise the performance of the ESP. Figure 1 shows the layout of a section of a typical GDP .

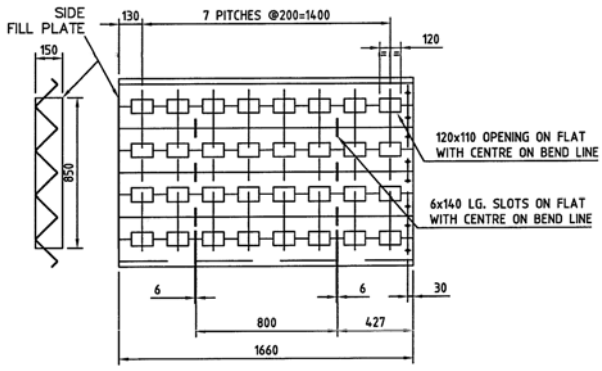

Figure 1: Detail of a portion of a Gas Distributor Plate.

Whether due to poor design or layout constraints, experience shows that inlet design is seldom ideal and some adjustment of the gas distributor plate apertures is necessary to optimise the ESP performance during commissioning. Unfortunately, prior to the advent of industrial CFD, the only means to achieve this was through iterative cycles of flow measurement and plate adjustment, with the latter only possible during prolonged system outage due to safety considerations.

The following analysis describes how CFD has been utilised to simulate and analyse the flow for 2 ESP's such that GDP's have been satisfactorily set-up prior to commissioning. The initial set-up was sufficient that no

re-adjustment of the GDP apertures was required and consequent down-time was eliminated entirely.

MODEL DESCRIPTION

Geometry

The subjects of the investigation were ESP's #5 and #7 of the Pinjarra upgrade project. Representations of the geometric models are shown in Figures 2 and 3. The ESP #7 inlet ductwork was designed with a shallow angle elbow, whereas the #5 system had to include the effects of an inlet flow swirl generated by an upstream cyclone and the effects of a perforated plate that was suggested by the ESP vendor. Beyond these, both systems have similar features including a steep angled inlet evase, the gas distributor plate, the ESP main body including electrodes, and an outlet contraction section.

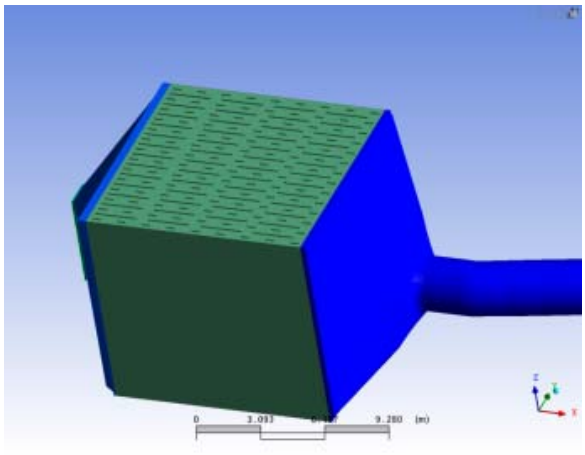

Figure 2: Model Geometry: ESP #7 and inlet duct.

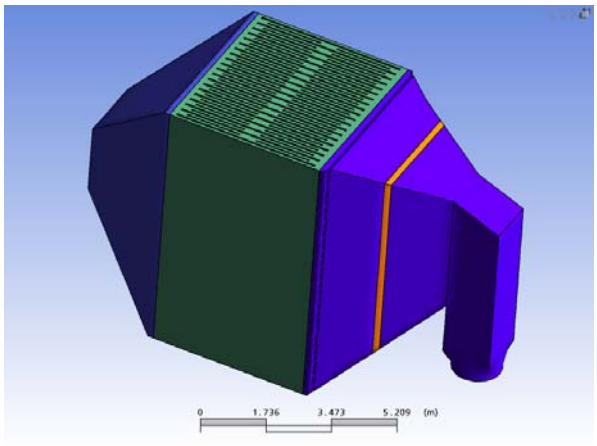

Figure 3: Model Geometry: ESP #5 and inlet duct.

A preliminary investigation showed that the ESP #7 displayed reasonable symmetry about the centre plane due to the insignificant effect of the initial elbow; ultimately only half of the #7 system was modelled. Unfortunately, no underlying symmetry exists for the #5 system as a consequence of the significant inlet swirl imparted by the upstream cyclone; the entire #5 system had to be modelled.

A slight simplification of the real geometry was used to model the gas distributor plate in which simple rectangular flow passages of 110 x 120 x 45 mm were used for each aperture. By so doing, the geometry generation could be automated in the native CAD (Solidedge v17) or grid pre-processor (ANSYS-Design Modeller), using a simple "pattern" function. Furthermore, changes to the geometry and grid for simulation of modified opening patterns of the GDP could be regenerated automatically after simply modifying a small number of control parameters.

Both models also used a slightly simplified geometric representation for the electrode array in which the electrode thickness was increased and the electrode spatial density reduced by a factor of 2. Because the focus of this work is on the inlet flow and because the effects of the electrode array are assumed to be negligible this approach was deemed adequate.

Grid

The native ANSYS-CFX meshing package was used to generate the computational grids for the two systems. In both cases the inlet and outlet sections used an unstructured tetrahedral element mesh. An extruded mesh comprised of prismatic and hex elements was used for the main body of the ESP. The "General Grid Interface" (GGI) approach was adopted at the inlet-ESP and ESP-outlet connection planes. The overall grid sizes were approximately 1,000,000 elements (450,000 nodes). A representative portion of the computational mesh is shown in Figure 4 (for clarity only the surface mesh has been shown).

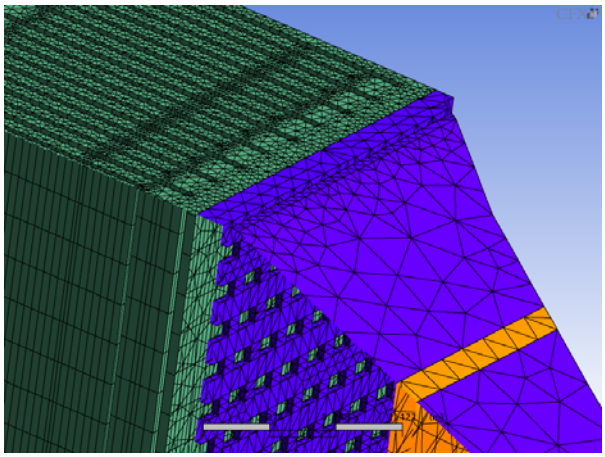

Figure 4: Computational Mesh: ESP #5.

Physical Models and Boundary Conditions

The essential features of the computational model followed a "standard" industrial approach for turbulent

flow (RANS equations, a standard k-epsilon turbulence model with wall functions (Launder and Spalding, 1974)) and there is no point in reproducing the governing equations here. The CFX standard "Higher-order differencing" scheme was used to reduce the effects of numerical diffusion particularly in view of the extensive use of tetrahedral mesh elements. In most cases CFX showed strong convergence behaviour with local momentum and mass residuals of less than 10^{-4} and global momentum and mass residuals of less than 0.1% within about 100 global iterations. Solutions for the ESP #5 were slightly less robust, presumably due to the inlet swirl boundary condition.

Only a single flow condition was considered for each of the ESP's. This corresponded to the normal operating conditions for the unit under consideration. Standard inlet turbulence quantities were assumed including 5% turbulence intensity and a turbulent/laminar viscosity ratio of 10. Details are given in Table 1.

		ESP #7	ESP #5
Inlet Normal Velocity	m/s	18.	38.
Inlet Swirl Velocity	m/s	na	38
Inlet turbulence intensity	%	5.	5.
Inlet turb. viscosity ratio	-	10.	10.
Mean Axial Velocity, ESP	m/s	1.	1.5
Gas Density	kg/m^3	0.66	0.55

Table 1: Boundary conditions.

RESULTS – ESP #7

The general flow characteristics in ESP #7 displayed a strong central jet impinging on the GDP, deflecting outwards and forming a toroidal vortex within the inlet evase. This resulted in a high lateral velocity (along the face of the GDP) at the mid-radial location. It is no surprise that the flow is unable to diffuse as rapidly as the steep angle of the inlet evase and the use of internal guide vanes within the evase would appear to be warranted. The GDP acts to reduce the intensity of the core of the jet, but a central bias still exists in the flow downstream of the GDP. Perhaps unexpectedly, there is a significant axial flow deficit predicted at the mid-radial position (corresponding to the region where the flow is moving laterally across the face of the GDP). At the periphery of the ESP the flow moves axially through the GDP and again establishes a region of locally higher velocity. The basic flow structure is shown in Figure 5.

A total of 5 configurations of GDP aperture openings were investigated with the basic goal of reducing the axial flow bias to the centre and periphery of the ESP. Ultimately it was found to be extremely difficult to promote mid-radial axial flow so for expediency the simplest modified setting was adopted. This required the closure of the outermost rows/ columns of apertures in the GDP to within 50% of their original open area and this set-up was used for commissioning.

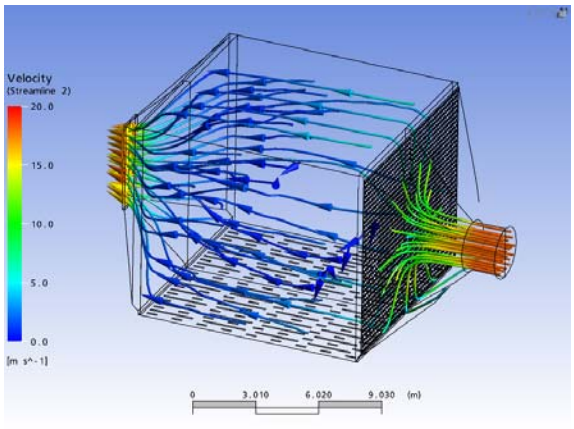

Figure 5: Flow structure, ESP #7.

The results of the various configurations were compared quantitatively during post-processing by calculating the percent cross sectional area in which the computed axial velocity is within +/- 50% of the desired mean at axial planes 1, 6, and 11 metres downstream of the GDP and on the vertical and horizontal centre-planes. The final results are summarised in Table 2.

Area % within +/- 50% of target velocity

CASE	Plane1	Plane 2	Plane 3	Centre Vert.	Centre Horiz.
Basecase	13	21	73	28	26
Final Mod	14	21	75	41	27

Table 2: Flow distribution results for the ESP #7.

RESULTS – ESP #5

A vertical inlet, significant inlet swirl, and the use of an upstream perforated plate resulted in significantly different flow behaviour for the ESP #5 system. Inlet swirl and the perforated plate both contribute significantly to a more uniform flow reaching the GDP. Similar to the #7 system, the flow is unable to diffuse as rapidly as the evase requires, which, in conjunction with the strong upward vertical flow at the inlet, generates a recirculation zone upstream of the distributor plate. A further similarity is the bias in the axial flow distribution downstream of the distributor plate at the point of initial jet impingement (in this case at the top of the ESP), an axial flow deficit where the inlet flow has turned and is directed parallel to the GDP. A second region of preferential axial flow is generated along the bottom perimeter of the ESP. The basic flow structure for ESP #5 is shown in Figure 6. A total of 5 runs were completed for ESP #5 including initial configurations without inlet swirl, without the upstream perforated plate, a basecase, and two cases with closures of selected sections of the GDP. The simulations confirmed the improved performance that could be achieved using a perforated plate upstream of the GDP and that, in this configuration, changes to the GDP porosity could only achieve very slight additional

improvements to this flow performance As a result the final recommendation for commissioning was to start up with the GDP in the fully open position.

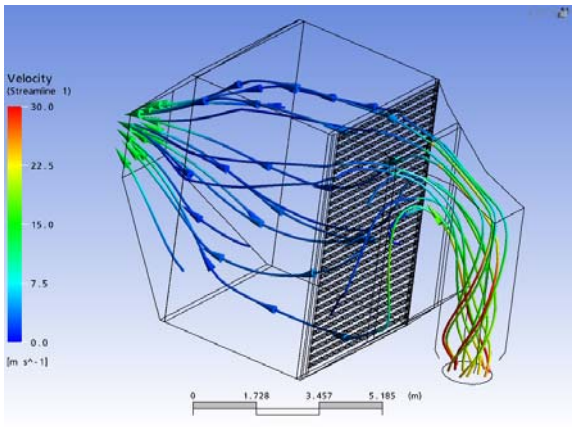

Figure 6: Flow structure, ESP #5.

COMPARISON WITH FIELD MEASUREMENTS

The GDP set-up for commissioning for the ESP 5 and 7 were as recommended from the above analyses. The first stage (cold-commissioning) includes a determination of satisfactory gas flow distribution by making a series of measurements in a rectangular grid pattern using a pitot-tube and manometer. The measurements are taken axially at a convenient position between electrode arrays.

There is considerable difficulty associated with the measurement of gas flows at the very low velocities and difficult conditions expected within the ESP. Errors arising from the lack of resolution of pressure measurements, uncertainties in positioning and/or non-alignment of the probe with the dominant flow direction, and inconsistencies in the signal processing have not been quantified here but are expected to be significant.

Unfortunately, field measurements taken on ESP #7 showed a significantly higher mean velocity than would be expected on the basis of the operating total flow rate or even the maximum possible ID fan output. This implied some fundamental calibration error for these measurements and although they seemed to suggest a reasonably uniform flow within the main body of the ESP, they were considered to be unreliable and have not been presented.

Measurements on ESP #5 provide a more reasonable benchmark of the computational model and are compared to the CFD results in Figure 7. The measurements indicate reasonable uniformity was achieved in the internal flow within the ESP and the measurements are in good agreement with the CFD predictions along the vertical centreline. However, the measurements do not demonstrate the top-bottom peripheral flow bias that was predicted by the CFD model.

The actual emission performance of both ESP's has been excellent without the need for further modification of the GDP settings beyond the initial set-up during cold commissioning. Stack samples taken downstream of ESP #7 have shown particulate levels well below the specified requirements of the unit.

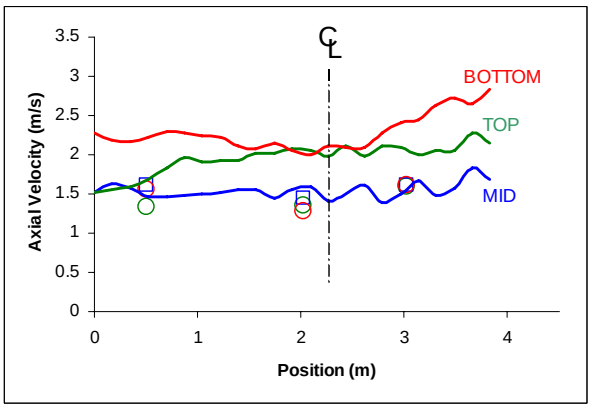

Figure 7: Field measurements (discrete points) and computations (solid lines) of axial velocity within ESP #5 approx 2.5 m downstream of GDP at vertical centreline, and at positions 0.5m from top and bottom of ESP.

MODEL DESCRIPTION – SUBDOMAIN APPROACH

While the current investigation has used CAD generated geometry and automated meshing to cope with the complexities of the GDP, a second approach (likely to have been used in the past) would be to approximate the effect of the GDP using a momentum source while explicitly modelling the remaining system geometry. This "subdomain" method, in which the GDP would be replaced by specified momentum source terms over a corresponding spatial region, is certainly appealing in terms of geometric simplification and reductions in grid size and solution time. Typically, the magnitude of the momentum sources would be determined on the basis of suitable correlations, such as that of Baines and Peterson (1951) as given in Equation 1. The fully open GDP has a porosity of 26.4%, so that the Baines and Peterson correlation (Equation 2) would suggest a loss coefficient (K) of 29., based on their suggested contraction coefficient of 0.6

$$\Delta P = K \frac{\rho V^2}{2} \qquad (1)$$

$$K = \left(\frac{(1 - C_c \varepsilon)}{C_c \varepsilon} \right)^2 \qquad (2)$$

As other investigators have done in the past (for example, Chen and Shirmer, 2003) the estimated loss coefficient was verified by detailed computation of the flow through an exact section of the GDP (in this case a single aperture). The detailed analysis indicated K = 24. in the Reynolds number range of interest, which is in reasonable agreement with the correlation. On this basis a subdomain model was developed for ESP #7 with the GDP simply represented as a region with specified momentum loss. Initially the loss was taken to be isotropic, however, even with a significantly increased

loss coefficient the resulting flow field failed to reproduce the results of the detailed model. The axial velocity contour plot along the centre plane (symmetry plane) for the detailed model is shown in Figure 8. Results with the simplified subdomain model using loss coefficients of 24 and 240 are shown in Figures 9 and 10. Neither shows the degree of peripheral flow or recirculation within the centre of the ESP that are predicted in the detailed model. Increasing the loss coefficient serves to distribute more evenly the incoming flow, but also significantly reduces the transverse flow. With increased loss coefficient (Figure 10) the flow emerging from the momentum loss subdomain becomes more and more aligned perpendicular to the GDP.

While it at first appealed intuitively that the loss due to the GDP should be isotropic, reference to the available literature (Shubauer et al, 1950, Carrothers and Baines, 1965, Sharan, 1975) indicated the opposite. In examining flow through thin screens at inclination angles up to 45 degrees, Shubauer et al. (1950) observed that the pressure drop was proportional to the square of the velocity component normal to the screen (known as the "cross-flow" principle). Hence, the pressure drop for transverse flows is effectively reduced by the square of the cosine of the approach angle. Subsequent work by Carrothers and Baines (1965) investigating screens at greater angles of inclination confirmed that loss coefficients generally followed the expected theoretical behaviour (ie the cross-flow principle) up to angles of approximately 60 degrees. Beyond this, the actual pressure drop exceeds the theoretical predictions. For example, the observed transverse loss factor at an incident angle of 85 degrees was 0.09 (versus 0.0075 according to the "cross-flow" estimate).

The use of an anisotropic loss subdomain model to represent the effects of the GDP provides better consistency with the results of the detailed model. Comparison of axial velocity contours between the detailed and subdomain models (Figure 8 and Figure 12 respectively) indicates similar peripheral flow bias and internal recirculation when the transverse loss is specified as 0.001 of the loss in the streamwise direction (in this case the "streamwise" direction is perpendicular to the GDP). The flow does not show a significant central recirculation zone until the transverse loss coefficient is less than 0.01 times the main streamwise loss coefficient.

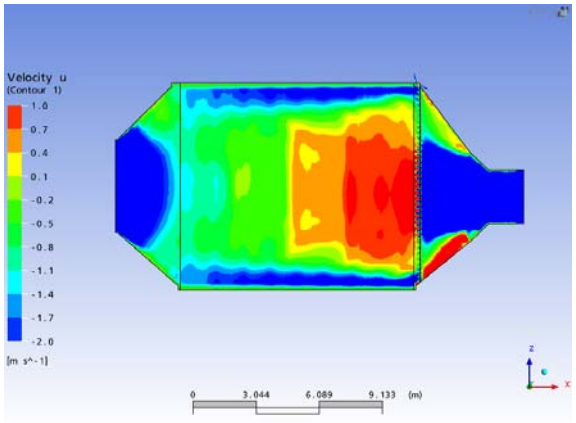

Figure 8:Axial velocity contours: Basecase, detailed model.

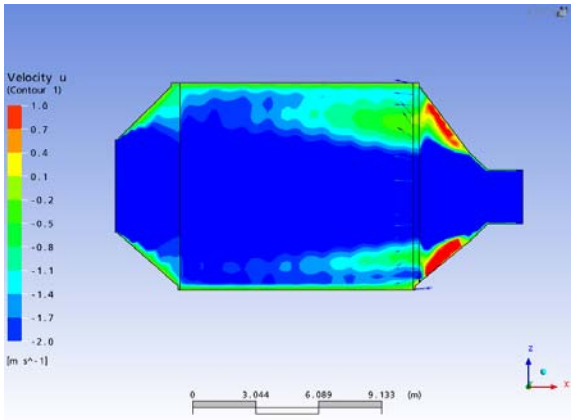

Figure 9: Axial velocity contours: Isotropic loss model K = 24.

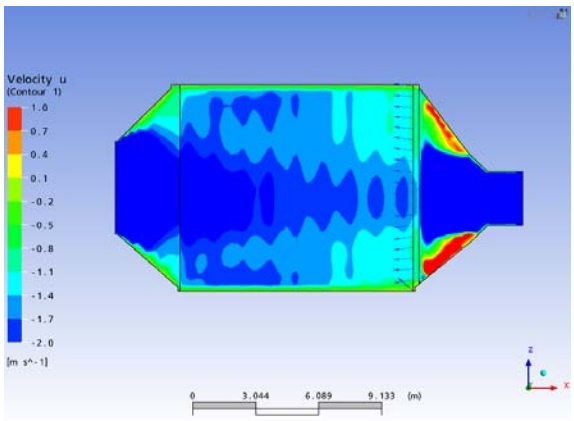

Figure 10: Axial velocity contours: Isotropic loss model K = 240.

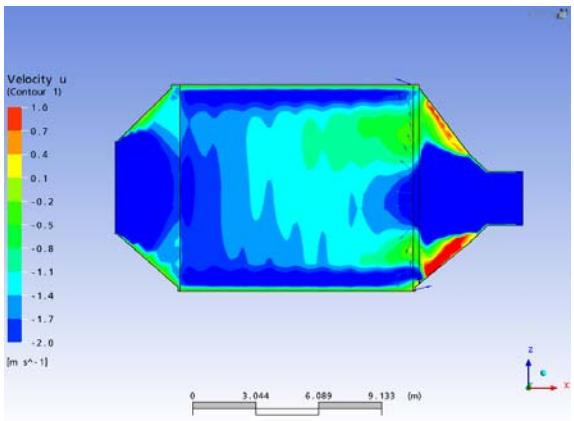

Figure 11: Axial velocity contours: Anisotropic loss model K = 24, transverse loss factor = 0.1

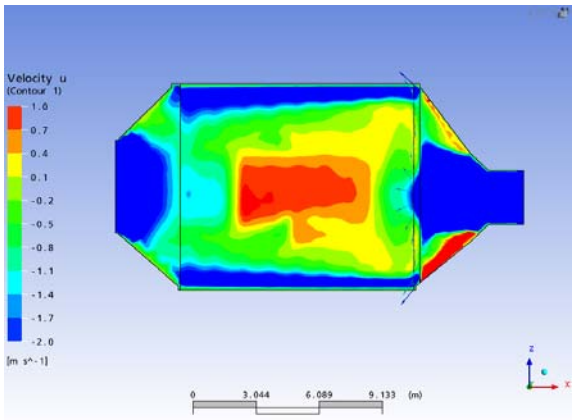

Figure 12: Axial velocity contours: Anisotropic loss model K = 24, transverse loss factor = 0.001

CONCLUSION

CFD modelling, in conjunction with CAD geometry development and automated grid generation, has been used to model the geometrically complex flow system in a modern ESP. The modelling was used to optimise the flow patterns within two ESP's as much as possible within the given constraints, such that further modification or set-up was not necessary following commissioning. The performance of the two ESP's continues to meet expectations. From a CFD modelling perspective the use of subdomain momentum loss models for these kinds of systems has considerable advantage. Unfortunately, the current work has been unable to provide guidance in the degree of anisotropy that the GDP momentum losses are likely to exhibit, and further investigation is required in this regard.

REFERENCES

LAUNDER, B.E. AND SPALDING, D.B (1974), "The numerical computation of turbulent flows". *Comp Meth Appl Mech Eng, 3:pp269-289*

BAINES W.D., and PETERSON E.G., (1951), "An Investigation of Flow through Screens", *Transactions of the ASME"*. July 1951, pp467-480.

CHEN M. and SCHIRMER K., (2003), "A Modelling Approach to the Design Optimization of Catalytic Converters of I.C. Engines", *Proceedings of ICEF03: 2003 Fall Technical Conference of the ASME Internal Combustion Engine Division"*. Sept 2003, pp467-480.

SCHUBAUER G.B., SPANGENBERG W.G., AND KLEBANOFF P.S., (1950), "Characteristics of Damping Screens", *NACA Technical Note 2001*, p1-39

CARROTHERS P.J.G. and BAINES W.D., (1965), "Forces on screens inclined to a fluid-flow", *Journal of Fluids Engineering - Transactions of the ASME*, V97 , n1, p116-117

SHARAN VK (1975), "Characteristics of Flow through 2-Dimensional Screens and Perforated Plates", *Journal of Scientific & Industrial Research*, V34, n2, p82-92